Noname manuscript No.
(will be inserted by the editor)

Modeling and control of head raising snake robots by using kinematic redundancy

Motoyasu Tanaka · Fumitoshi Matsuno

Received: date / Accepted: date

Abstract In this paper, we consider trajectory tracking control of a head raising snake robot on a flat plane by using kinematic redundancy. We discuss the motion control requirements to accomplish trajectory tracking and other tasks, such as singular configuration avoidance and obstacle avoidance, for the snake robot. The features of the internal motion caused by kinematic redundancy are considered, and a kinematic model and a dynamic model of the snake robot are derived by introducing two types of shape controllable point. The first is the head shape controllable point, and the other is the base shape controllable point. We analyzed the features of the two kinds of shape controllable point and proposed a controller to accomplish the trajectory tracking of the robot's head as its main task along with several sub-tasks by using redundancy. The proposed method to accomplish several sub-tasks is useful for both the kinematic model and the dynamic model. Experimental results using a head raising snake robot which can control the angular velocity of its joints show the effectiveness of the proposed controller.

Keywords Snake robots · redundancy · trajectory tracking · head raising

1 Introduction

Snakes can travel in various environments, e.g., on uneven terrain, on walls, underwater, and on trees, despite their simple limbless bodies [1,2]. Snake robots are robots which imitate snakes and have long and thin bodies, and these robots are expected to be actively used in search and rescue operations in pipes and at disaster sites [3–5]. Snakes travel by using the features of their bodies, which make it hard for them to sideslip. There are two types of articulated mobile robots like

M. Tanaka
The University of Electro-Communications, 1-5-1 Chofugaoka, Chofu, Tokyo, Japan
Tel.: +81-42-443-5430
Fax: +81-42-443-5430
E-mail: mtanaka@uec.ac.jp

F. Matsuno
Kyoto University, Kyotodaigakukatsura, Nishikyo-ku, Kyoto 606-8530, Japan.

snakes. The first is the articulated robot, which has slim body and moves by using a different propulsion mechanism than snakes, e.g., active wheels or crawlers [3–6]. The other is the snake robot which moves by using the difference of frictional forces like snakes [7,1,8–21]. Snake robots have many joints and move by using friction. It is therefore difficult to operate snake robots. This paper considers the control of snake robots for more effective operation.

Previous studies proposed the control of snake robots based on observations from biology [1], a continuum approximation [14,15], a decentralized approach [16–18], and model based control [9–11]. Hirose has long investigated snake robots and has produced several snake robots, and he models snakes by using a wheeled link mechanism (where passive wheels are attached at the side of the snake robot's body) with no side slip [1]. He defined the *serpenoid curve* and achieved snake robot locomotion by an undulating motion similar to that of real snakes. Using this approach, the robot can be moved by the simple input to the joints, but it is difficult to carry out complicated tasks, e.g., trajectory tracking. The continuum approximation [14,15] is a more generalized approach than the serpenoid curve. The joint inputs can be calculated with respect to an arbitrary continuum curve, but discretization errors occur if the inputs are applied to the snake robot, because the robot is not continuous and has discrete links. In the decentralized approach [16–18], the joint inputs are simple and effective and adaptive movements were accomplished. This approach is interesting but it is unsuitable for position and tracking control applications because the desired position, direction, and velocity of the motion are not available in this method. Thus, these approaches are not suitable for high-precision motion or complicated tasks. These tasks, e.g., trajectory tracking, can be accomplished by a model-based approach. In this approach, it is necessary for the snake robot to avoid singular configurations [8].

For two-dimensional (2D) snake robots, we find that the introduction of links without wheels and shape controllable points (SCPs; these are the directly controllable angles corresponding to the wheelless links in the snake robot's body) makes the system redundancy controllable, based on a kinematic model [9]. We proposed a trajectory tracking controller based on a kinematic model [9] and a dynamic model [10]. Using the proposed control laws and by controlling the shape controllable points, the robot can accomplish trajectory tracking of its head position without converging into a singular configuration. The shape controllable points mean that the joint angles can be controlled to adjust the shape of the snake robot [10].

For three-dimensional (3D) snake robots, Ma derived a model that considered Coulomb friction for interaction with the environment and developed a simulator [12], and also discussed the head-raising motion of snake robots based on the serpenoid curve [13]. Date and Takita proposed a continuum model for 3D snake-like creeping locomotion and a control method based on discretization of the optimal bending moment [14]. Kamegawa proposed an operation method using helical rolling [19]. In addition, for control of snake robots in 3D discrete environments, methods based on a continuum approximation [22] and on piecewise differentiable gaits [20] have also been proposed. However, in these studies, there is no discussion of the trajectory tracking control of the snake's head.

A snake robot is similar to a mobile manipulator [23] when some of the top links (i.e. the head part) of the robot are lifted up from the ground. In this case, the head part of the snake can act like the hand of a manipulator. However, a snake robot

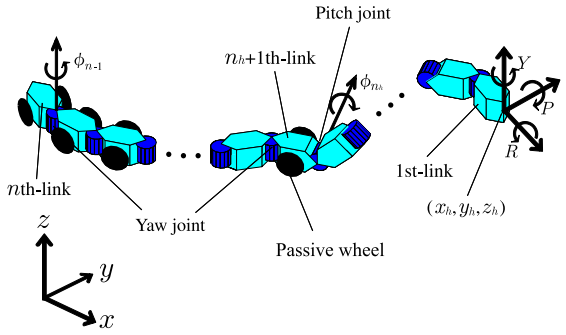

Fig. 1 An n-link head raising snake robot

is essentially different to a mobile manipulator. Although a mobile manipulator has two separate mechanisms to accomplish its locomotion and manipulation tasks independently, a snake robot has two functions, locomotion and manipulation, and it can change these functions adaptively. A snake robot can accomplish various complicated tasks by using redundancy, and an example of such a task has been discussed in the literature [21].

In this paper, we consider a trajectory tracking controller for a head raising snake robot that can accomplish several sub-tasks by using kinematic redundancy. A popular approach for control of a redundant manipulator is to control the internal dynamics related to the kinematic redundancy by using the basis of the internal motion [24]. The same approach can be applied to the snake robot. In this approach, deriving the basis matrix and then obtaining its differential are very difficult, especially for a complicated nonlinear system like a snake robot. We therefore consider the features of the internal motion caused by kinematic redundancy and introduce shape controllable point [9,10] to the dynamic model of the head raising snake robot. By using kinematic redundancy, we propose a trajectory tracking controller which also accomplishes several sub-tasks. Experiments were carried out to demonstrate the effectiveness of the proposed control method.

2 Model

We consider an n link, wheeled, head raising snake robot, as shown in Fig. 1. All wheels are passive and all joints are active, and we assume that a passive wheel does not slide in the side direction. The length of the links are $2l$, the wheels are attached at the central point of the link, and the distance between the center of the link and the center of the wheel is l_w[m]. For simplicity, let us define the head part as being constructed from the first link to the n_h-th link, the base part as being from the n_h+1-th to the n-th link and the compositions of the head and base parts do not change. The number of links of the head part is n_h and that of the base part is n_b. We introduce the following assumptions at the modeling stage.

[Assumption 1]: Each joint rotates around the pitch or yaw axis.
[Assumption 2]: All joints of the base part rotate around the yaw axis, and the

connected joint between the head and the base part rotates around the pitch axis.
[Assumption 3]: The environment is flat.
[Assumption 4]: The robot is supported by the wheels of the base part and the head part is not in contact with the ground.
[Assumption 5]: The $n_h + 1$-th link (the top link of the base part) is wheeled.
[Assumption 6]: The base part is constrained to the environment and the robot does not fall over.

Based on Assumptions 1–4, all wheels of the base part are in contact the environment and the head part can move without being constrained by the environment. Assumption 5 was introduced to separate the head part and the base part clearly. Assumption 6 was introduced to simplify the model.

The flat environment corresponds to the xy plane of the inertial coordinate system O-xyz. Let $\boldsymbol{w} = [x_h, y_h, z_h, R, P, Y]^T$ (roll-pitch-yaw convention) be the position and attitude of the snake head with respect to O-xyz. Let $\boldsymbol{\phi} = [\phi_1, \cdots, \phi_{n-1}]^T$ be the set of relative joint angles, and let $\boldsymbol{\tau} = [\tau_1, \cdots, \tau_{n-1}]^T$ be the set of joint torques. Let us define $\boldsymbol{q} = [\boldsymbol{w}^T, \boldsymbol{\phi}^T]^T \in \mathbf{R}^{n+5}$. The position and attitude of the snake head has 6 degrees of freedom (DOF) and the base joint of the head part can only move on a 2D plane, because the movement of the base part is constrained on the xy plane. Therefore, the head part must have at least four joints or four links to accomplish an arbitrary position and attitude for the snake head. Kinematic redundancy occurs by increasing the number of head links, and the DOFs of the kinematic redundancy m_h is $m_h = n_h - 4$.

In the case where all links of the base part are wheeled and we assume that a passive wheel does not slide in the sideways direction, the kinematic equation based on the velocity constraint for passive wheels is expressed as follows [25]:

$$A(\boldsymbol{q})\dot{\boldsymbol{w}} = B(\boldsymbol{q})\dot{\boldsymbol{\phi}} \tag{1}$$

where $A \in \mathbf{R}^{(n_b+3)\times 6}$, $B \in \mathbf{R}^{(n_b+3)\times(n-1)}$,

$$B = \begin{bmatrix} b_{11} & \cdots & b_{1n_h} & & & \mathbf{0} \\ b_{21} & \cdots & b_{2n_h} & -l & & \\ \vdots & & \vdots & & \ddots & \\ b_{n_b1} & \cdots & b_{n_bn_h} & b_{n_b(n_h+1)} & \cdots & -l \\ b_{(n_b+1)1} & \cdots & b_{(n_b+1)n_h} & 0 & \cdots & 0 \\ b_{(n_b+2)1} & \cdots & b_{(n_b+2)n_h} & 0 & \cdots & 0 \\ b_{(n_b+3)1} & \cdots & b_{(n_b+3)n_h} & 0 & \cdots & 0 \end{bmatrix}. \tag{2}$$

Consider a snake robot where m_b passive wheels corresponding to the $i_1, \cdots, i_{m_b}$-th links are removed, and let us define $m = m_h + m_b$, and the kinematic equation based on the velocity constraint for passive wheels is expressed as

$$\bar{A}(\boldsymbol{q})\dot{\boldsymbol{w}} = \bar{B}(\boldsymbol{q})\dot{\boldsymbol{\phi}}. \tag{3}$$

By transforming the equation, we obtain

$$\dot{\boldsymbol{\phi}} = \bar{B}^{\dagger}\bar{A}\dot{\boldsymbol{w}} + \mathcal{N}(\boldsymbol{q})\boldsymbol{\eta} \tag{4}$$

where $\bar{A}(\boldsymbol{q}) \in \mathbf{R}^{(n_b-m_b+3)\times 6}$ and $\bar{B}(\boldsymbol{q}) \in \mathbf{R}^{(n_b-m_b+3)\times(n-1)}$ are the matrices where the corresponding $i_1, \cdots, i_{m_b}$-th row vectors are eliminated from the original matrices A and B respectively, $\bar{B}^{\dagger}$ is the pseudo inverse matrix of $\bar{B}$, $\mathcal{N}(\boldsymbol{q}) \in \mathrm{Ker}(\bar{B})$

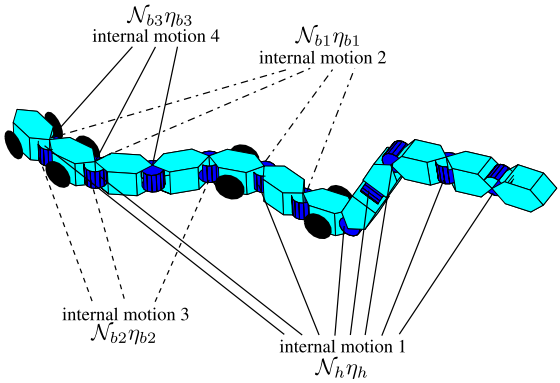

Fig. 2 The internal motion caused by removing the wheels of the 12-link snake robot

and $\boldsymbol{\eta} = [\boldsymbol{\eta}_h^T,\ \boldsymbol{\eta}_b^T]^T \in \mathbf{R}^m$, $\boldsymbol{\eta}_h \in \mathbf{R}^{m_h}$, $\boldsymbol{\eta}_b = [\eta_{b1}, \cdots, \eta_{bm_b}]^T \in \mathbf{R}^{m_b}$. $\mathcal{N}$, with rows that span the null space of $\bar{B}$, is the basis matrix for the internal motion which does not affect the motion of $\dot{\boldsymbol{w}}$, and $\boldsymbol{\eta}$ is the total internal motion and $\boldsymbol{\eta}_b$ and $\boldsymbol{\eta}_h$ are the parts of the internal motion that are related to the base part and the head part, respectively. The internal motion is caused by the kinematic redundancy of the robot. The kinematic redundancy of type "redundancy II" (where the number of constraint equations is less than the number of inputs: $n_b - m_b + 3 < n - 1$) is defined in [9]. The number of the internal motion of the snake robot increases by increasing the number of links in the head part and removing wheels from the base part, and we obtain $\mathcal{N}\boldsymbol{\eta} = \mathcal{N}_h\boldsymbol{\eta}_h + \mathcal{N}_b\boldsymbol{\eta}_b$.

A popular approach for the control of a redundant manipulator is to control the internal dynamics related to the kinematic redundancy by using a basis matrix $\mathcal{N}$ of the internal motion [24]. In the case where we apply this approach to complicated nonlinear systems such as snake robots, derivation of the basis matrix and obtaining its differential are difficult. We therefore treat the SCP as the representation of the redundancy [9,10].

From the structure of $\bar{B}$, the basis matrix $\bar{\mathcal{N}}$, which has row vectors that span the null space of $\bar{B}$, is expressed as

$$\bar{\mathcal{N}} = \begin{bmatrix} \bar{\boldsymbol{v}}_{1h} & & \cdots & & \bar{\boldsymbol{v}}_{(n-1)h} \\ 0 \cdots 0 & \bar{v}_{(i_1-1)1} & & \cdots & \bar{v}_{(n-1)1} \\ \vdots & & \ddots & & \vdots \\ 0 \quad \cdots & & 0 & \bar{v}_{(i_{m_b}-1)m_b} \cdots & \bar{v}_{(n-1)m_b} \end{bmatrix}^T \tag{5}$$

where $\bar{\boldsymbol{v}}_{ih} \in \mathbf{R}^{m_h}$. By performing operations involving deleting and adding the column vectors of (5), we derive the basis matrix $\mathcal{N}$ of the internal motion. It is

expressed as

$$
\begin{aligned}
\mathcal{N} &= [\mathcal{N}_h \ | \ \mathcal{N}_b] \\
&= [\mathcal{N}_h \ | \ \mathcal{N}_{b1} \ \mathcal{N}_{b2} \ \cdots \ \mathcal{N}_{bm_b}] \\
&= \left[\begin{array}{c|cccc}
\boldsymbol{v}_{1h} & 0 & 0 & \cdots & 0 \\
\vdots & \vdots & & & \\
\boldsymbol{v}_{(i_1-2)h} & 0 & & & \\
 & & \vdots & & \\
\boldsymbol{0} & v_{(i_1-1)(m_h+1)} & & & \\
\boldsymbol{v}_{i_1 1} & v_{i_1(m_h+1)} & & & \\
\vdots & \vdots & & & \vdots \\
\boldsymbol{v}_{(i_2-2)h} & v_{(i_2-2)(m_h+1)} & 0 & & \\
\boldsymbol{0} & 0 & v_{(i_2-1)(m_h+2)} & & \\
\boldsymbol{v}_{i_2 h} & v_{i_2(m_h+1)} & v_{i_2(m_h+2)} & & \\
\vdots & \vdots & \vdots & \ddots & \\
\boldsymbol{v}_{(i_{m_b}-2)h} & v_{(i_{m_b}-2)(m_h+1)} & v_{(i_{m_b}-2)(m_h+2)} & & 0 \\
\boldsymbol{0} & 0 & 0 & & v_{(i_{m_b}-1)m} \\
\boldsymbol{v}_{i_{m_b}h} & v_{i_{m_b}(m_h+1)} & v_{i_{m_b}(m_h+2)} & & v_{i_{m_b}m} \\
\vdots & \vdots & \vdots & & \vdots \\
\boldsymbol{v}_{(n-1)h} & v_{(n-1)(m_h+1)} & v_{(n-1)(m_h+2)} & \cdots & v_{(n-1)m}
\end{array}\right]
\end{aligned}
\tag{6}
$$

where $\boldsymbol{v}_{ih} \in \mathbf{R}^{1\times m_h} (i = 1, \cdots, n-1)$.

From (6), we find that $\mathcal{N}_{bj}\eta_{bj}$ $(j=1, \cdots, m_b)$ affects $\dot{\phi}_{i_j-1}$ and $\dot{\phi}_k$ $(k > i_j\text{–}1,\ k \neq i_j - 1, \cdots, i_{m_b} - 1)$. $\dot{\phi}_{i_j-1}$ is the joint velocity corresponding to the j-th wheelless link and $\dot{\phi}_k$ corresponds to the wheeled link which is posterior to the j-th wheelless link. Note that $\mathcal{N}_b\boldsymbol{\eta}_b$ does not affect the velocities of joints which are anterior to the joint velocity $\dot{\phi}_{i_1}$ corresponding to the first wheelless link. The joint angles ϕ_{i_j-1} of the wheelless link of the base part are introduced into the controlled variables $\boldsymbol{w}$ as a representation of the kinematic redundancy of the base part [9]. In this paper, we call $\tilde{\boldsymbol{\phi}}_b = [\tilde{\phi}_{b1}, \cdots, \tilde{\phi}_{bm_b}]^T = [\phi_{i_1-1}, \cdots, \phi_{i_{m_b}-1}]^T \in \mathbf{R}^{m_b}$ the "base shape controllable point" (B-SCP). These representations seem to be appropriate because the B-SCPs have one-to-one relationships with each internal motion $\boldsymbol{\eta}_b$ of the base part and the number of B-SCPs is equal to the degree of $\boldsymbol{\eta}_b$.

On the other hand, $\mathcal{N}_h\boldsymbol{\eta}_h$, caused by the redundant links of the head part, affects the velocities of all joints except the B-SCPs $\tilde{\boldsymbol{\phi}}_b$. Because the degree of internal motion $\boldsymbol{\eta}_h$ of the head part is m_h, we introduce the m_h joint angles of the head part $\tilde{\boldsymbol{\phi}}_h = [\tilde{\phi}_{h1}, \cdots, \tilde{\phi}_{hm_h}]^T \in \mathbf{R}^{m_h}$ into the variables to be controlled $\boldsymbol{w}$ as a representation of the kinematic redundancy of the head part. We call $\tilde{\boldsymbol{\phi}}_h$ the "head shape controllable point" (H-SCP).

For example, Fig. 2 shows the internal motion of a 12-link snake robot, where $n_h = 5$, $n_b = 7$, and the wheels of the 7th, 9th and 10th links are removed. In this case, the internal motion is $\boldsymbol{\eta} = [\eta_h, \eta_{b1}, \eta_{b2}, \eta_{b3}]^T \in \mathbf{R}^4$, $m_b = 3$, $m_h = 1$, and $\mathcal{N}$

is described as

$$\mathcal{N} = [\mathcal{N}_h \ | \ \mathcal{N}_b] = [\mathcal{N}_h \mid \mathcal{N}_{b1}\ \mathcal{N}_{b2}\ \mathcal{N}_{b3}]$$
$$= \left[\begin{array}{c|ccc} v_{1h} & 0 & 0 & 0 \\ v_{2h} & & & \\ v_{3h} & \vdots & \vdots & \vdots \\ v_{4h} & & & \\ v_{5h} & 0 & 0 & 0 \\ 0 & v_{6b_1} & 0 & 0 \\ v_{7h} & v_{7b_1} & 0 & 0 \\ 0 & 0 & v_{8b_2} & 0 \\ 0 & 0 & 0 & v_{9b_3} \\ v_{10h} & v_{10b_1} & v_{10b_2} & v_{10b_3} \\ v_{11h} & v_{11b_1} & v_{11b_2} & v_{11b_3} \end{array}\right].$$

Therefore, the B-SCPs are $\tilde{\boldsymbol{\phi}}_b = [\phi_6, \phi_8, \phi_9]^T$, and the H-SCP is one of the joint angles of the head part.

We set all the SCPs as $\tilde{\boldsymbol{\phi}} = [\tilde{\boldsymbol{\phi}}_h^T,\ \tilde{\boldsymbol{\phi}}_b^T]^T \in \mathbf{R}^m$, the vector except $\tilde{\boldsymbol{\phi}}$ from $\boldsymbol{\phi}$ as $\bar{\boldsymbol{\theta}} \in \mathbf{R}^{n-m-1}$, and the state variables to be controlled as $\tilde{\boldsymbol{w}} = [\boldsymbol{w}^T, \tilde{\boldsymbol{\phi}}^T]^T$. The kinematic equation (3) is thus rewritten as

$$\tilde{A}(\boldsymbol{q})\dot{\tilde{\boldsymbol{w}}} = \tilde{B}(\boldsymbol{q})\dot{\bar{\boldsymbol{\theta}}} \tag{7}$$

By multiplying $\tilde{B}^{-1}$ from the left hand side of the above equation, we obtain

$$\dot{\bar{\boldsymbol{\theta}}} = \bar{F}\dot{\tilde{\boldsymbol{w}}} = \bar{F}_1\dot{\boldsymbol{w}} + \bar{F}_2\dot{\tilde{\boldsymbol{\phi}}}_h + \bar{F}_3\dot{\tilde{\boldsymbol{\phi}}}_b \tag{8}$$

where $\bar{F} = \tilde{B}^{-1}\tilde{A} = [\bar{F}_1 \ \ \bar{F}_2 \ \ \bar{F}_3] \in \mathbf{R}^{(n-m-1)\times(6+m)}$. We set the joint angles of the head part except for the H-SCP to be $\bar{\boldsymbol{\theta}}_h \in \mathbf{R}^{n_h-m_h}$, and the joint angles of the base part except for the B-SCP are $\bar{\boldsymbol{\theta}}_b \in \mathbf{R}^{n_b-m_b-1}$, and

$$\dot{\bar{\boldsymbol{\theta}}} = [\dot{\bar{\boldsymbol{\theta}}}_h^T \ \ \dot{\bar{\boldsymbol{\theta}}}_b^T]^T \tag{9}$$
$$= \left[\begin{array}{c} \bar{F}_{1h} \\ \bar{F}_{1b} \end{array}\right]\dot{\boldsymbol{w}} + \left[\begin{array}{c} \bar{F}_{2h} \\ \bar{F}_{2b} \end{array}\right]\dot{\tilde{\boldsymbol{\phi}}}_h + \left[\begin{array}{c} \boldsymbol{0} \\ \bar{F}_{3b} \end{array}\right]\dot{\tilde{\boldsymbol{\phi}}}_b \tag{10}$$

where $\bar{F}_{1h} \in \mathbf{R}^{(n_h-m_h)\times 6}$, $\bar{F}_{1b} \in \mathbf{R}^{(n_b-m_b-1)\times 6}$, $\bar{F}_{2h} \in \mathbf{R}^{(n_h-m_h)\times m_h}$, $\bar{F}_{2b} \in \mathbf{R}^{(n_b-m_b-1)\times m_h}$, and $\bar{F}_{3b} = [\bar{F}_{3b1}, \cdots, \bar{F}_{3bm_b}]^T \in \mathbf{R}^{(n_b-m_b-1)\times m_b}$.

In this case, we provide the following conditions.

[Condition 1]: The tail link is wheeled.
[Condition 2]: The directions of the rotational axes of all joints of the head part are not the same.
[Condition 3]: The H-SCPs are selected so that the directions of the rotational axes of all joints of the head part, except for the H-SCPs, are not the same.
[Condition 4]: $1 \leq m < n - 7$.
[Condition 5]: $n_h \geq 4$.

Conditions 1–3 are necessary conditions to ensure full rank of the matrix $\tilde{B}$, Condition 4 means that "the dimension of the state vector to be controlled $(6+m)$ is less than the dimension of the input vector $(n-1)$, i.e. $6 + m < n - 1$", and ensures that the kinematic redundancy of the system is $m > 1$. Condition 5 is necessary to achieve arbitrary positioning and attitude for the snake head.

2.1 Kinematic model

We set the input $\boldsymbol{u}$ to be $\dot{\boldsymbol{\phi}}$ and the controlled variable is $\tilde{\boldsymbol{w}}$. From eq.(3), the kinematic model of the snake robot can be expressed as follows:

$$\hat{A}(\boldsymbol{q})\dot{\tilde{\boldsymbol{w}}} = \hat{B}(\boldsymbol{q})\boldsymbol{u} \tag{11}$$

$$\hat{A} = \begin{bmatrix} \bar{A} & \boldsymbol{0} \\ \boldsymbol{0} & I_m \end{bmatrix} \in \mathbf{R}^{(n-1)\times(6+m)}$$

$$\hat{B} = \begin{bmatrix} & \bar{B} & \\ \bar{h}_{11} & \cdots & \bar{h}_{1(n-1)} \\ \vdots & & \vdots \\ \bar{h}_{m_h 1} & \cdots & \bar{h}_{m_h(n-1)} \\ \bar{b}_{11} & \cdots & \bar{b}_{1(n-1)} \\ \vdots & & \vdots \\ \bar{b}_{m_b 1} & \cdots & \bar{b}_{m_b(n-1)} \end{bmatrix} \in \mathbf{R}^{(n-1)\times(n-1)}$$

$$\bar{h}_{ks} = \begin{cases} 1 & \text{if } \ s = j_k \\ 0 & \text{otherwise} \end{cases}$$

$$\bar{b}_{ks} = \begin{cases} 1 & \text{if } \ s = i_k \\ 0 & \text{otherwise} \end{cases}$$

The kinematic redundancy is expressed via the SCPs in eq. (11) and we can use the redundancy by design of the desired value of the SCPs.

2.2 Dynamics

We consider the velocity constraints with respect to the generalized coordinates. We set the selection matrices $S \in \mathbf{R}^{(m+6)\times(n+5)}$, $\bar{S} \in \mathbf{R}^{(n-m-1)\times(n+5)}$, which select $\tilde{\boldsymbol{w}}$ and $\bar{\boldsymbol{\theta}}$ from $\boldsymbol{q}$, to be as per the following equations.

$$\tilde{\boldsymbol{w}} = S\boldsymbol{q}, \ \bar{\boldsymbol{\theta}} = \bar{S}\boldsymbol{q} \tag{12}$$

where $SS^T = I_{m+6}$, $\bar{S}\bar{S}^T = I_{n-m-1}$, $S\bar{S}^T = 0$. The relationship between $\tilde{\boldsymbol{w}}$, $\bar{\boldsymbol{\theta}}$ and $\boldsymbol{q}$ is then expressed as

$$\boldsymbol{q} = T \begin{bmatrix} \tilde{\boldsymbol{w}} \\ \bar{\boldsymbol{\theta}} \end{bmatrix} \tag{13}$$

$$T = [S^T \ \ \bar{S}^T] \in \mathbf{R}^{(n+5)\times(n+5)}$$

where $T^{-1} = T^T$. From (8) and (13), the following equation is derived for the velocity constraints with respect to generalized coordinates.

$$[-\bar{F} \ \ I_{n-m-1}]T^T\dot{\boldsymbol{q}} = \boldsymbol{0} \tag{14}$$

By considering (14) and introducing the Lagrange multiplier $\boldsymbol{\lambda}$, the dynamics of the snake robot are obtained as follows:

$$M(\boldsymbol{q})\ddot{\boldsymbol{q}} + h(\boldsymbol{q}, \dot{\boldsymbol{q}}) + \tilde{g}(\boldsymbol{q}) + T \begin{bmatrix} -\bar{F}^T \\ I_{n-m-1} \end{bmatrix} \boldsymbol{\lambda} = E\boldsymbol{\tau} \tag{15}$$

$$E = \begin{bmatrix} O_{6\times(n-1)} \\ I_{n-1} \end{bmatrix} \in \mathbf{R}^{(n+5)\times(n-1)}$$

where $M(\boldsymbol{q}) \in \mathbf{R}^{(n+5)\times(n+5)}$ is an inertial matrix, $h(\boldsymbol{q}, \dot{\boldsymbol{q}}) \in \mathbf{R}^{(n+5)\times 1}$ is the coriolis, centrifugal and viscous term, $\tilde{g}(\boldsymbol{q})$ is the gravity term, and $\boldsymbol{\tau}$ is the input torque. By multiplying (15) by $[I_{m+6} \quad \bar{F}^T]T^T$ from the left-hand side, we obtain the following equation.

$$\bar{M}\ddot{\boldsymbol{q}} + \bar{h} = \tilde{E}\boldsymbol{\tau} \tag{16}$$

where

$$\begin{aligned} \bar{M} &= [I_{m+6} \quad \bar{F}^T]T^T M \in \mathbf{R}^{(m+6)\times(n+5)} \\ \bar{h} &= [I_{m+6} \quad \bar{F}^T]T^T(h + \tilde{g}) \in \mathbf{R}^{(m+6)\times 1} \\ \tilde{E} &= [I_{m+6} \quad \bar{F}^T]T^T E \in \mathbf{R}^{(m+6)\times(n-1)}. \end{aligned} \tag{17}$$

Also, from (8) and (13), we obtain

$$\dot{\boldsymbol{q}} = T \begin{bmatrix} I_{m+6} \\ \bar{F} \end{bmatrix} \dot{\tilde{\boldsymbol{w}}} \tag{18}$$

$$\ddot{\boldsymbol{q}} = T \begin{bmatrix} I_{m+6} \\ \bar{F} \end{bmatrix} \ddot{\tilde{\boldsymbol{w}}} + T \begin{bmatrix} O_{m+6} \\ \dot{\bar{F}} \end{bmatrix} \dot{\tilde{\boldsymbol{w}}} \tag{19}$$

By substituting (19) in (16), we obtain the dynamic equation for the head raising snake robot with respect to $\tilde{\boldsymbol{w}}$ as follows.

$$\tilde{M}\ddot{\tilde{\boldsymbol{w}}} + \tilde{h} = \tilde{E}\boldsymbol{\tau} \tag{20}$$

where

$$\begin{aligned} \tilde{M} &= [I_{m+6} \quad \bar{F}^T]T^T M T \begin{bmatrix} I_{m+6} \\ \bar{F} \end{bmatrix} \in \mathbf{R}^{(m+6)\times(m+6)} \\ \tilde{h} &= [I_{m+6} \quad \bar{F}^T]T^T(h + \tilde{g}) \\ &\quad + [I_{m+6} \quad \bar{F}^T]T^T M T \begin{bmatrix} O_{m+6} \\ \dot{\bar{F}} \end{bmatrix} \dot{\tilde{\boldsymbol{w}}} \in \mathbf{R}^{(m+6)\times 1}. \end{aligned}$$

3 Control design for the main objective

Using feedback linearization, let us define the control input $\boldsymbol{\tau}$ as

$$\boldsymbol{\tau} = \tilde{E}^{\dagger}\{\tilde{M}(\ddot{\tilde{\boldsymbol{w}}}_d - K_v\dot{\boldsymbol{e}} - K_p\boldsymbol{e}) + \tilde{h}\} + \boldsymbol{\tau}_{ker} \tag{21}$$

where $\tilde{E}^{\dagger}$ is a pseudo inverse matrix of $\tilde{E}$, $\boldsymbol{e} = \tilde{\boldsymbol{w}} - \tilde{\boldsymbol{w}}_d$, and $\boldsymbol{\tau}_{ker}$ is an arbitrary vector which satisfies $\boldsymbol{\tau}_{ker} \in \mathrm{Ker}(\tilde{E})$. By selecting $K_v, K_p > 0$, $\tilde{\boldsymbol{w}}$ converges to the desired vector $\tilde{\boldsymbol{w}}_d$. $\boldsymbol{\tau}_{ker}$ is the term caused by the dynamic redundancy defined as "redundancy I" (where the dimension of the state vector to be controlled $(6 + m)$ is less than the dimension of the input vector $(n-1)$) in [9]. The kinematic redundancy is represented by the SCPs $\tilde{\boldsymbol{\phi}}$, which are included in $\tilde{\boldsymbol{w}}$, and we can use the kinematic redundancy by appropriate design of the desired value $\tilde{\boldsymbol{\phi}}_d$.

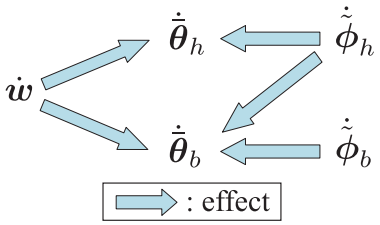

Fig. 3 The relationship among $\dot{\boldsymbol{q}}$ values of a head raising snake robot

The aforementioned controller is a torque controller based on feedback linearization. However, the proposed method involves the design of the desired velocity of the SCPs by using kinematic redundancy. It is therefore possible to perform control based on a kinematic model using the desired velocity obtained by the proposed method. We design the control input $\boldsymbol{u}$ with respect to the kinematic model (11) as

$$\boldsymbol{u} = \hat{B}^{-1}\hat{A}\{\dot{\tilde{\boldsymbol{w}}}_d - K(\tilde{\boldsymbol{w}} - \tilde{\boldsymbol{w}}_d)\} \tag{22}$$

where $K > 0$ is a feedback gain. The closed loop system is then

$$\hat{A}\left\{\dot{\tilde{\boldsymbol{w}}} - \dot{\tilde{\boldsymbol{w}}}_d + K(\tilde{\boldsymbol{w}} - \tilde{\boldsymbol{w}}_d)\right\} = \boldsymbol{0}. \tag{23}$$

If $\hat{A}$ is a row of full rank, i.e., the robot is not in a singular configuration, $\tilde{\boldsymbol{w}}$ converges to $\tilde{\boldsymbol{w}}_d$ when $t \to \infty$ because the solution of (23) is given as

$$\dot{\tilde{\boldsymbol{w}}} - \dot{\tilde{\boldsymbol{w}}}_d + K(\tilde{\boldsymbol{w}} - \tilde{\boldsymbol{w}}_d) = \boldsymbol{0} \tag{24}$$

and $(\tilde{\boldsymbol{w}} - \tilde{\boldsymbol{w}}_d)$ is exponentially stable.

4 Control design for the sub-objectives

4.1 Desired value

We consider increases in the values of some cost functions as sub-tasks. We proposed a control strategy that can ensure the convergence of the velocities of the SCPs to their desired values to accomplish the increase/decrease of a cost function $V(\boldsymbol{q})$ by using the whole kinematic redundancy [10]. However, if there are multiple degrees of kinematic redundancy, we may be able to achieve several sub-tasks without the need for trade-offs for each sub-task.

From section 2, the relationship between the $\dot{\boldsymbol{q}}$ values is shown as Fig. 3. Note that the velocity of the H-SCP $\dot{\tilde{\boldsymbol{\phi}}}_h$ effects $\dot{\tilde{\boldsymbol{\theta}}} = [\dot{\tilde{\boldsymbol{\theta}}}_h^T, \dot{\tilde{\boldsymbol{\theta}}}_b^T]^T$ and the velocity of the B-SCP $\dot{\tilde{\boldsymbol{\phi}}}_b$ does *not* effect $\dot{\bar{\boldsymbol{\theta}}}_h$. Therefore, the sub-task of the H-SCP can be accomplished independently of the base part by setting the cost function $V_h(\boldsymbol{w}, \tilde{\boldsymbol{\phi}}_h, \bar{\boldsymbol{\theta}}_h)$, which does not depend on the joint angles of the base part. Let us define the desired values of the H-SCP $\dot{\tilde{\boldsymbol{\phi}}}_{hd}$ as

$$\dot{\tilde{\boldsymbol{\phi}}}_{hd} = a_h \left(\frac{\partial V_h}{\partial \tilde{\boldsymbol{\phi}}_h} + \frac{\partial V_h}{\partial \bar{\boldsymbol{\theta}}_h} \bar{F}_{2h} \right)^T \tag{25}$$

where $a_h > 0$ is an appropriate gain coefficient. In the case where the H-SCP converges to the desired values, by considering (10), the time derivative of the cost function $V_h(\boldsymbol{w}, \tilde{\boldsymbol{\phi}}_h, \bar{\boldsymbol{\theta}}_h)$ can be expressed approximately as

$$\begin{aligned}\dot{V}_h &= \frac{\partial V_h}{\partial \boldsymbol{w}}\dot{\boldsymbol{w}} + \frac{\partial V_h}{\partial \tilde{\boldsymbol{\phi}}_h}\dot{\tilde{\boldsymbol{\phi}}}_h + \frac{\partial V_h}{\partial \bar{\boldsymbol{\theta}}_h}\dot{\bar{\boldsymbol{\theta}}}_h \\ &\simeq \left(\frac{\partial V_h}{\partial \boldsymbol{w}} + \frac{\partial V_h}{\partial \bar{\boldsymbol{\theta}}_h}\bar{F}_{1h}\right)\dot{\boldsymbol{w}}_d \\ &\quad + a_h\left(\frac{\partial V_h}{\partial \tilde{\boldsymbol{\phi}}_h} + \frac{\partial V_h}{\partial \bar{\boldsymbol{\theta}}_h}\bar{F}_{2h}\right)\left(\frac{\partial V_h}{\partial \tilde{\boldsymbol{\phi}}_h} + \frac{\partial V_h}{\partial \bar{\boldsymbol{\theta}}_h}\bar{F}_{2h}\right)^T. \end{aligned} \tag{26}$$

Because the first term of the right hand side of (26) does not depend on $\dot{\tilde{\boldsymbol{\phi}}}_h$ and the second term of the right hand side is non-negative, then controlling the H-SCP $\dot{\tilde{\boldsymbol{\phi}}}_h$ to converge to the desired values $\dot{\tilde{\boldsymbol{\phi}}}_{hd}$ makes the cost function V_h increase. It can not ensure that $\dot{V}_h$ becomes positive but can contribute to an increase of V_h like a manipulator [26].

Next, we consider the base part. We set the cost function $V_b(\boldsymbol{q})$, which should be increased by using the B-SCP $\tilde{\boldsymbol{\phi}}_b$, and we define the desired velocity of the B-SCP $\dot{\tilde{\boldsymbol{\phi}}}_{bd}$ as

$$\dot{\tilde{\boldsymbol{\phi}}}_{bd} = a_b\left(\frac{\partial V_b}{\partial \tilde{\boldsymbol{\phi}}_b} + \frac{\partial V_b}{\partial \bar{\boldsymbol{\theta}}_b}\bar{F}_{3b}\right)^T \tag{27}$$

where $a_b > 0$ is a gain coefficient. In the case where the B-SCPs converge to the desired values, the time derivative of the cost function $V_b(\boldsymbol{q})$ can be expressed approximately as

$$\begin{aligned}\dot{V}_b &= \frac{\partial V_b}{\partial \boldsymbol{w}}\dot{\boldsymbol{w}} + \frac{\partial V_b}{\partial \tilde{\boldsymbol{\phi}}_h}\dot{\tilde{\boldsymbol{\phi}}}_h + \frac{\partial V_b}{\partial \tilde{\boldsymbol{\phi}}_b}\dot{\tilde{\boldsymbol{\phi}}}_b + \frac{\partial V_b}{\partial \bar{\boldsymbol{\theta}}}\dot{\bar{\boldsymbol{\theta}}} \\ &\simeq \left(\frac{\partial V_b}{\partial \boldsymbol{w}} + \frac{\partial V_b}{\partial \bar{\boldsymbol{\theta}}}\bar{F}_1\right)\dot{\boldsymbol{w}}_d + \left(\frac{\partial V_b}{\partial \tilde{\boldsymbol{\phi}}_h} + \frac{\partial V_b}{\partial \bar{\boldsymbol{\theta}}}\bar{F}_2\right)\dot{\tilde{\boldsymbol{\phi}}}_{hd} \\ &\quad + a_b\left(\frac{\partial V_b}{\partial \tilde{\boldsymbol{\phi}}_b} + \frac{\partial V_b}{\partial \bar{\boldsymbol{\theta}}_b}\bar{F}_{3b}\right)\left(\frac{\partial V_b}{\partial \tilde{\boldsymbol{\phi}}_b} + \frac{\partial V_b}{\partial \bar{\boldsymbol{\theta}}_b}\bar{F}_{3b}\right)^T. \end{aligned} \tag{28}$$

The first and second terms in (28) do not depend on $\dot{\tilde{\boldsymbol{\phi}}}_b$, and the third term contributes the increase in V_b because it is non-negative. The second term in (28) is the effect of the H-SCP, and the H-SCP interferes with the sub-task of the B-SCP. However, this problem can be solved by appropriate adjustment of a_b.

Consequently, by controlling the SCPs as discussed above, the snake robot can then accomplish two sub-tasks, which are the increases in V_h and V_b, simultaneously.

4.2 Cost function

The manipulability is important because the head part of the robot is mainly used for the manipulation task. Increasing the manipulability of the kinematic model

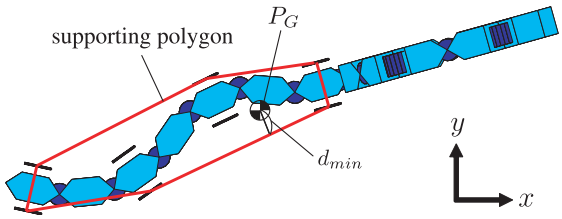

Fig. 4 The supporting polygon of the snake robot

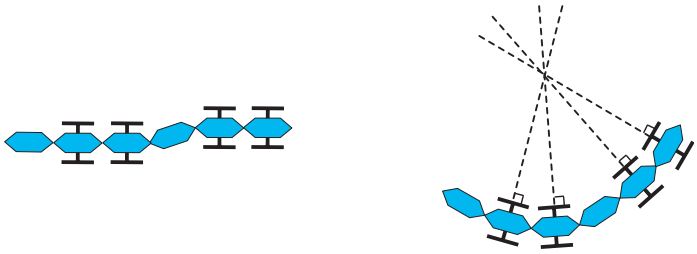

Fig. 5 Singular configurations of the snake robot

(7) is therefore regarded as a sub-task of the head part. We set the cost function $V_h(\boldsymbol{w}, \tilde{\boldsymbol{\phi}}_h, \bar{\boldsymbol{\theta}}_h)$ of the head part to be

$$V_h(\boldsymbol{w}, \tilde{\boldsymbol{\phi}}_h, \bar{\boldsymbol{\theta}}_h) = \det(\tilde{B}). \tag{29}$$

It is necessary for the snake robot to avoid a singular configuration where all the passive wheels are either parallel or in an arc shape, as shown in Fig. 5, because the input torque diverges if the snake robot converges to a singular configuration [8]. Thus, we regard singularity avoidance as a sub-task of the base part. When $\tilde{E}$ in (20) is not of full rank, the robot is in the singular configuration [10]. Also, the snake robot may possibly fall down. If the robot falls down, Assumption 6 is then not satisfied. As shown in Fig. 4, the snake robot is statically stable when the projective point P_G of the robot's center of mass in the environment is contained within the supporting polygon of the grounded wheels. We set the cost function $V_b(\boldsymbol{q})$ of the base part corresponding to $\tilde{\boldsymbol{\phi}}_b$ to be

$$\begin{aligned} V_b(\boldsymbol{q}) &= a' V_{b1} + b' V_{b2} \\ &= a' \det(\tilde{E}\tilde{E}^T) + b' d_{min} \end{aligned} \tag{30}$$

where a' and b' are non-negative constants and d_{min} is the distance from P_G to the supporting polygon. The robot can avoid the singular configuration and reduce the risk of falling by simply increasing the value of the above cost function. $\hat{A}$ will no longer be of full rank, along with $\tilde{E}$, if the robot is in a singular configuration. Thus, the robot can avoid the singular configuration by ensuring that $\det(\tilde{E}\tilde{E}^T) \neq 0$ in the case of kinematic model based control. The robot can accomplish several sub-tasks based on the kinematic model by setting $\dot{\tilde{\boldsymbol{\phi}}}_d$ as per (25) and (27) in the input (22).

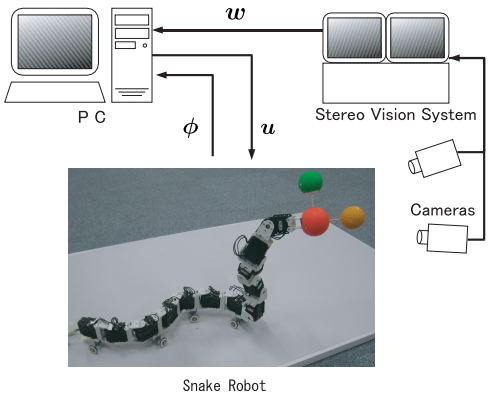

Fig. 6 Experimental system

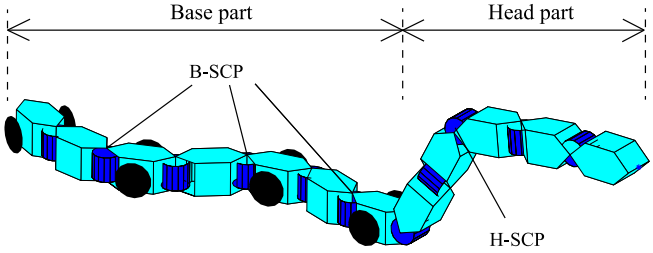

Fig. 7 The experimental model of the head raising snake robot

5 Experiments

Experiments have been conducted to demonstrate the effectiveness of the proposed control law. The experimental system is shown in Fig. 6. The controlled robot is a 12-link snake robot, where $n_h = 5$, $n_b = 7$, $m_h = 1$, $m_b = 3$, $l = 0.034$ [m] and $l_w = 0.032$ [m]. As shown in Fig. 7, the first, third and fifth links have pitch joints, while the other links have yaw joints, and the seventh, ninth and eleventh links are wheelless. We set values for the H-SCP $\tilde{\phi}_h = \phi_3$, the B-SCP $\tilde{\boldsymbol{\phi}}_b = [\tilde{\phi}_{b1}, \tilde{\phi}_{b2}, \tilde{\phi}_{b3}]^T = [\phi_6, \phi_8, \phi_{10}]^T$, and $\tilde{\boldsymbol{w}} = [\boldsymbol{w}^T, \phi_3, \phi_6, \phi_8, \phi_{10}]^T$. The actuators used were *Dynamixel AX-12* by Robotis. The controller was implemented on a computer, where the CPU is a Pentium IV operating at 3 GHz and the operating system is Windows XP. The position and attitude of the robot were measured using *Quick MAG IV*, which is a stereo vision system manufactured by Ohyoh Keisoku Kenkyusho.

We considered the following three control methods.
[Case 1]: Kinematic redundancy is not used and the desired velocities of all SCPs are set to zero.
[Case 2]: The sub-task corresponding to the H-SCP is set as an increase in the static manipulability and the sub-task corresponding to the B-SCP is set as singularity avoidance.
[Case 3]: The sub-task corresponding to the H-SCP is again set as an increase in

Table 1 Initial configurations and desired trajectories for experiments

$\boldsymbol{\phi}(0)$	$[-0.11, 0, 0, 0, 1.1, \frac{-\pi}{9}, \frac{\pi}{6}, \frac{\pi}{6}, \frac{-\pi}{9}, \frac{-\pi}{6}, \frac{-\pi}{10}]^T$
$\boldsymbol{w}_d$	$[0.01t, 0, 0.2, \frac{\pi}{8}, \frac{\pi}{8}, 0]^T$
K	$\mathrm{diag}(0.4, 0.25, 0.5, 0.1, 0.1, 0.1, 0, 0, 0, 0)$

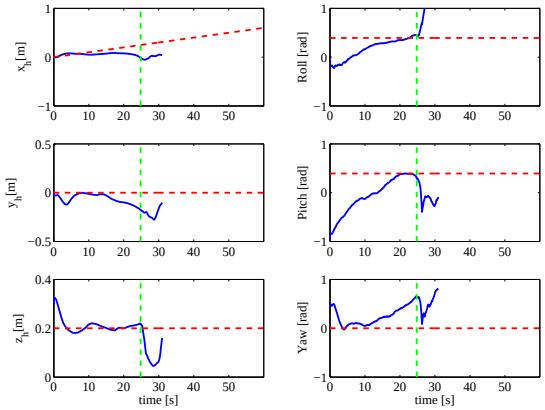

Fig. 8 Time responses of $\boldsymbol{w}$ for experimental Case 1

the static manipulability and the sub-task corresponding to the B-SCP is set as avoidance of both singular configurations and falls.
In Case 2 and Case 3, we set the desired velocity of the H-SCP as per (25), with $a_h = 1.0 \times 10^5$, and the desired velocity of the B-SCP as per (27), with $a_b = 1$. In Case 2, $a' = 1.0 \times 10^{-11}$ and $b' = 0$. In Case 3, $a' = 1.0 \times 10^{-11}$ and $b' = 3.0$. The experimental parameters and the desired trajectories are shown in Table 1.

Figures 8–14 show the experimental results. Figures 8–10 show the responses of $\boldsymbol{w}$ in each case and a broken line represents the desired trajectory in each case. Figures 11–14 show the responses of $\boldsymbol{u}$, $\bar{\boldsymbol{\theta}}$, $\tilde{\boldsymbol{\phi}}$, the cost functions $V_h = \det(\tilde{B})$, $V_{b1} = \det(\tilde{E}\tilde{E}^T)$ and $V_{b2} = d_{min}$ in each case, and Fig. 15 shows the motion of the snake robot in Case 3. In all figures, broken vertical lines represent the times when the robots fell down in Case 1 and Case 2.

In Case 1, V_{b1} became zero as shown in Fig. 14, which is the singular configuration, and x_h thus did not track the desired trajectory, as shown in Fig. 8. The robot fell down at $t = 24.8$ [s] because V_{b2} reached the neighborhood of zero and the experiment was stopped at $t = 31.0$ [s].

In Case 2, V_{b1} did not converge to zero, as shown in Fig. 14, because the SCPs vibrated periodically, as shown in Fig. 13. Thus, the robot was able to avoid the singularity. Note that the robot was not given the periodic reference explicitly but the periodic motion was spontaneously caused based on the cost function. From Figs. 9 and 13, the trajectory tracking of $\boldsymbol{w}$ and the increase in V_h, which is the sub-task of the H-SCPs, are seen to be accomplished before the robot falls down. However, V_{b2} decreased to almost zero and the robot fell down at $t = 45.7$ [s], as shown in Fig 14.

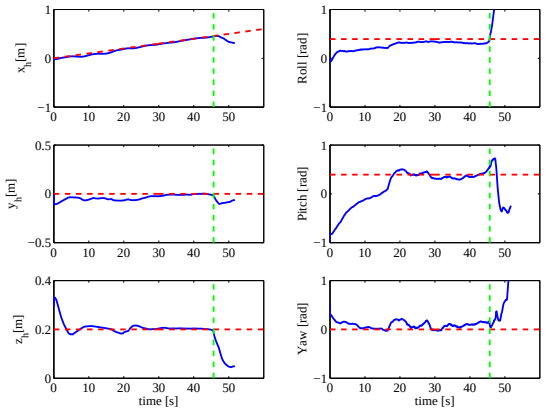

Fig. 9 Time responses of $\boldsymbol{w}$ for experimental Case 2

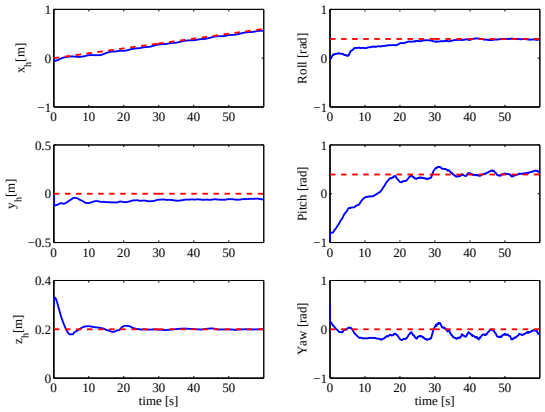

Fig. 10 Time responses of $\boldsymbol{w}$ for experimental Case 3

However, in Case 3, the robot did not fall down because V_{b2} increased, as shown in Fig. 14. From Figs. 13 and 14, we can see that the increases in V_h and V_{b1} were accomplished. However, there was a small steady-state error in y_h, even while the response of the other controlled variable almost tracked the desired trajectory, as shown in Fig. 10. We believe that the cause of this error was a modeling error caused by the sideslip of the wheels, because the input velocity $\boldsymbol{u}$ of Case 3 was larger than that of the other cases, as shown in Fig. 11. The difference in the input velocity between the cases is caused by the existence or non-existence of the avoidance of falls.

The more posterior that the angle of the base part was, then the larger the wave motion of that angle became in Case 2. This motion may be suitable for a straight trajectory because this motion is similar to the motion of fish. The motion in Case 3 was different to the motion in Case 2 because of the trade-off between singularity avoidance and fall avoidance.

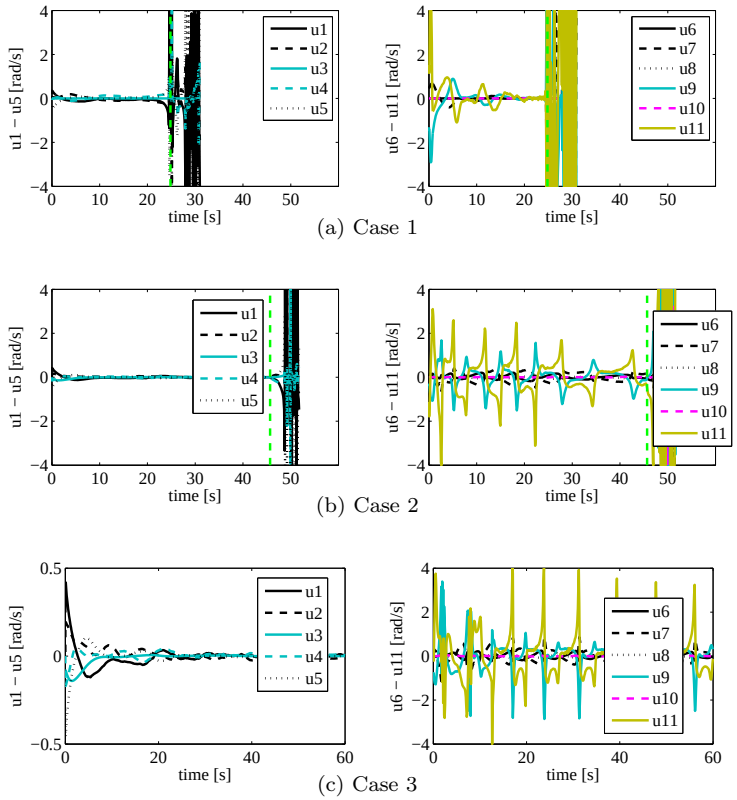

Fig. 11 Time responses of $\boldsymbol{u}$ from the experiments

From the experiments, it was found that the proposed controller for the head raising snake robot is effective for a velocity-controlled robot.

6 Conclusions

This paper proposed a control method for trajectory tracking of a head raising snake robot on a plane. The proposed controller can accomplish trajectory tracking of the robot's head, with several sub-tasks, by using the features of kinematic redundancy, where the motions of the B-SCPs do not affect the motion of the head part. Experiments demonstrated the effectiveness of the proposed controller for a velocity-controlled robot based on the kinematic model.

In future studies, we will consider the case where the environment is not planar, and operation by using the raised head of the robot like the end-effector of a manipulator. In this paper, the joints which are used for the SCPs are fixed. We will also study how to select the joints for use as the SCPs and how to use these SCPs to accomplish the sub-tasks more effectively.

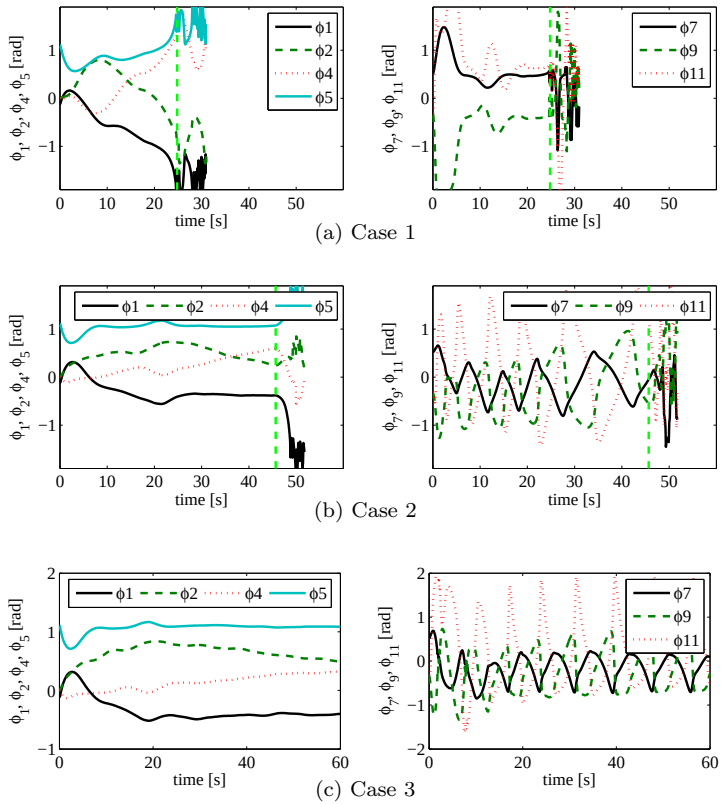

Fig. 12 Time responses of $\bar{\boldsymbol{\theta}}$ from the experiments

References

1. Hirose, S.: Biologically Inspired Robots: Snake-like Locomotor and Manipulator. Oxford University Press (1993)
2. Gans, C.: Biomechanics: An Approach to Vertebrate Biology. The University of Michigan Press (1974)
3. Kamegawa, T., Yamasaki, T., Igarashi, H., Matsuno, F.: Development of the snake-like rescue robot KOHGA. Proc. IEEE Int. Conf. on Robotics and Automation. 5081-5086 (2004)
4. Osuka, K., Kitajima, H.: Development of mobile inspection robot for rescue activities: MOIRA. Proc. IEEE/RSJ Int. Conf. on Intelligent Robots and Sys. 3373-3377 (2002)
5. Arai, M., Tanaka, Y., Hirose, S., Kuwahara, H., Tsukui, S.: Development of "Souryu-IV" and Souryu-V:" serially connected crawler vehicles for in-rubble searching operations. J. of Field Robotics. 25, 31-65 (2008)
6. Borestein, J., Hansen, M., Borrell, A.: The OmniTread OT-4 serpentine robot–design and performance. J. of Field Robotics. 24, 601-621 (2007)
7. Mori, M., Hirose, S.: Three-dimensional serpentine motion and lateral rolling by active cord mechanism ACM-R3. Proc. IEEE/RSJ Int. Conf. on Intelligent Robots and Sys. 829-834 (2002)
8. Prautsch, P., Mita, T., Iwasaki, T.: Analysis and control of a gait of snake robot. Trans. IEEJ. 120-D, 372-381 (2000)

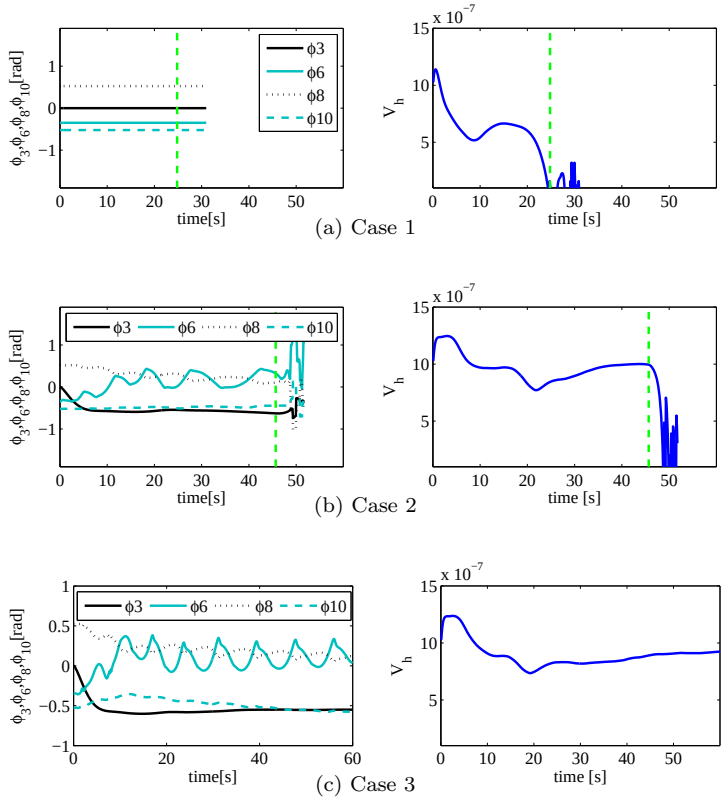

Fig. 13 Time responses of $\tilde{\phi}$ and V_h from the experiments

9. Matsuno, F., Mogi, K.: Redundancy controllable system and control of snake robot with redundancy based on kinematic model. Proc. IEEE Conf. on Decision and Control. 4791-4796 (2000)
10. Matsuno, F., Sato, H.: Trajectory tracking control of snake robot based on dynamic model. Proc. IEEE Int. Conf. on Robotics and Automation. 3040-3046 (2005)
11. Liljebäck, P., Pettersen, K.Y., Stavdahl, Ø., Gravdahl, J.T.: Snake Robots (Modelling, Mechatronics, and Control). Springer, London (2013)
12. Ma, S., Ohmameuda, Y., Inoue, K.: Dynamic analysis of 3-dimensional snake robots. Proc. IEEE/RSJ Int. Conf. on Intelligent Robots and Sys. 767-772 (2004)
13. Ye, C., Ma, S., Li, B., Wang, Y.: Head-raising motion of snake-like robots. Proc. IEEE Int. Conf. on Robotics and Biomimetics. 595-600 (2004)
14. Date, H., Takita, Y.: Control of 3D snake-like locomotive mechanism based on continuum modeling. Proc. ASME2005 Int. Design Eng. Technical Conf. No. DETC2005-85130 (2005)
15. Yamada, H., Hirose, S.: Study on the 3D shape of active cord mechanism. Proc. IEEE Int. Conf. on Robotics and Automation. 2890-2895 (2006)
16. Kano, T., Sato, T., Ishiguro, R.: Decentralized control of scaffold-assisted serpentine locomotion that exploits body softness. Proc. IEEE Int. Conf. on Robotics and Automation, 5129-5134 (2011)
17. Sato, T., Kano, T., Ishiguro, A.: A snake-like robot driven by a decentralized control that enables both phasic and tonic control. Proc. IEEE/RSJ Int. Conf. on Intelligent Robots and Sys. 1881-1886 (2011)

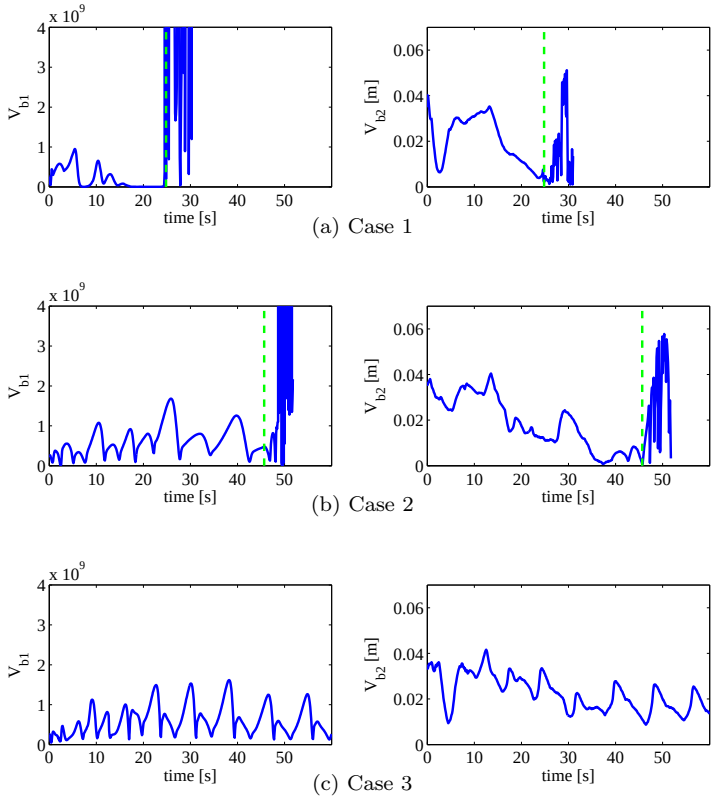

Fig. 14 Time responses of V_b from the experiments

18. Kano, T., Sato, T., Kobayashi, R., Ishiguro, A.: Decentralized control of multi-articular snake-like robot for efficient locomotion. Proc. IEEE/RSJ Int. Conf. on Intelligent Robots and Sys. 1875-1880 (2011)
19. Kamegawa, T., Baba, T., Gofuku, A.: V-shift control for snake robot moving the inside of a pipe with helical rolling motion. Proc. IEEE Int. Symp. on Safety, Security and Rescue Robotics. 1-6 (2011)
20. Lipkin, K., Brown, I., Peck, A., Choset, H., Rembisz, J., Gianfortoni, P., Naaktgeboren, A.: Differentiable and piecewise differentiable gaits for snake robots. Proc. IEEE/RSJ Int. Conf. on Intelligent Robots and Sys. 1864-1869 (2007)
21. Tanaka, M., Matsuno, F.: Cooperative control of two snake robots. Proc. IEEE Int. Conf. on Robotics and Automation. 400-405 (2006)
22. Takaoka, S., Yamada, H., Hirose, S.: Snake-like active wheel robot ACM-R4.1 with joint torque sensor and limiter. Proc. IEEE/RSJ Int. Conf. on Intelligent Robots and Sys. 1081-1086 (2011)
23. Yamamoto, Y., Yun, X.: Effect of the dynamic interaction on coordinated control of mobile manipulators. IEEE Trans. on Robotics and Automation. 12, 5, 816-824 (1996)
24. Murray, R., Li, Z., Sastry, S.: A Mathematical Introduction to Robotic Manipulation. CRC Press, Boca Raton (1994)
25. Matsuno F., Suenaga, K.: Control of Redundant 3D Snake Robot based on Kinematic Model. Proc IEEE Int. Conf. on Robotics and Automation. 2061-2066 (2003)
26. Yoshikawa T.: Analysis and Control of Robot Manipulators with Redundancy. Robotics Research: The First International Symposium. 735-747 (1984)

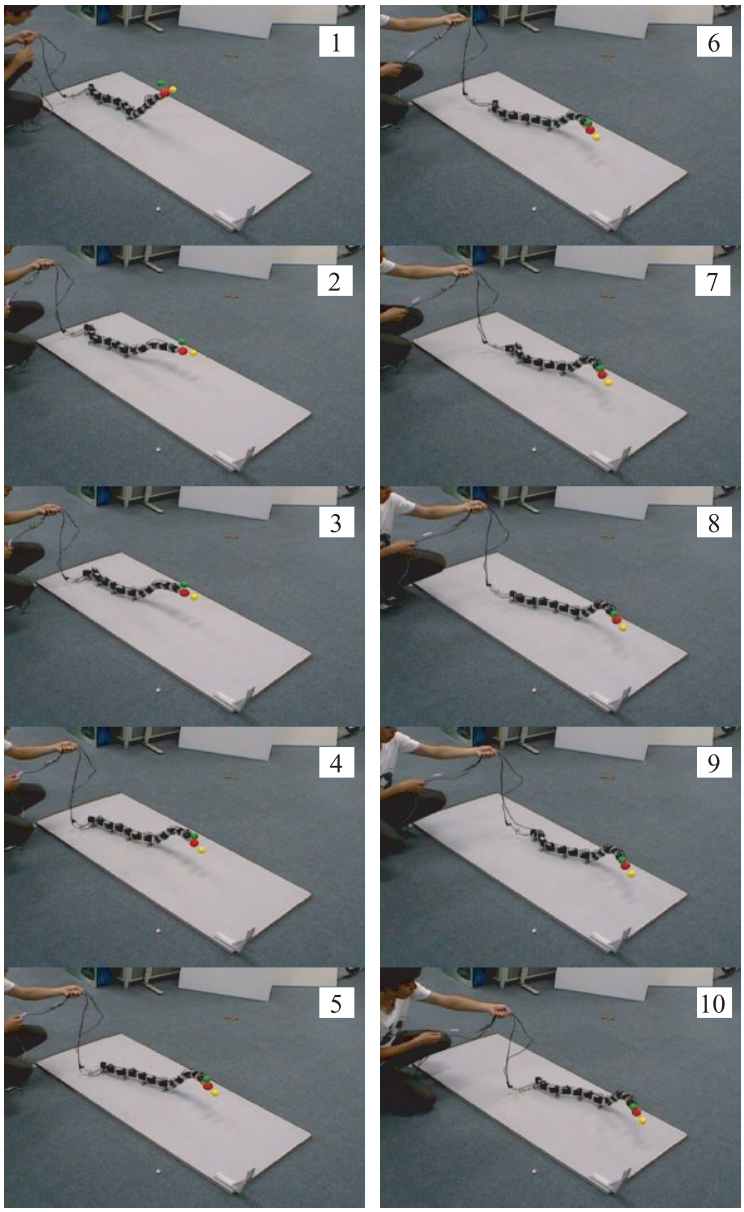

Fig. 15 The motion of the snake robot in experimental Case 3